RAPID COMMUNICATIONS

910 nm vertical-cavity surface-emitting laser arrays with 100 W output power level and low driving current

Japanese Journal of Applied Physics **57**, 100302 (2018)
https://doi.org/10.7567/JJAP.57.100302

RAPID COMMUNICATION

910 nm vertical-cavity surface-emitting laser arrays with 100 W output power level and low driving current

Jianwei Zhang[1], Yongqiang Ning[1], Xing Zhang[1]*, Werner Hofmann[2], Kefu Liu[3,4], Jun Zhang[1], Jian Qiu[3,4], Yugang Zeng[1], Xihong Fu[1], Youwen Huang[1,5], Lei Xiang[1,5], Yingying Liu[1,5], Jiye Zhang[1,4], Li Qin[1], and Lijun Wang[1]

[1]*State Key Laboratory of Luminescence and Applications, Changchun Institute of Optics, Fine Mechanics and Physics, Chinese Academy of Sciences, Changchun 130033, China*
[2]*Technical University of Berlin, Berlin 10623, Germany*
[3]*Academy for Engineering and Technology, Fudan University, Shanghai 200433, China*
[4]*Engineering Research Center of Advanced Lighting Technology, Ministry of Education, Fudan University, Shanghai 200433, China*
[5]*University of Chinese Academy of Sciences, Beijing 100049, China*

*E-mail: zhangx@ciomp.ac.cn

Received May 24, 2018; accepted July 16, 2018; published online August 28, 2018

In this paper, we present monolithic 910 nm high-power vertical-cavity surface-emitting laser (VCSEL) arrays with addressable sectors suitable for long-distance light detection and ranging (LIDAR). The peak output power of a single VCSEL array (163 devices) reaches 25.5 W under 30-ns-pulse operation. The peak power of the larger sectored 2×2 VCSEL array reaches 100 W at an operating current of 55 A. To the best of our knowledge, this is the first report on achieving a 100 W output power level with a 910 nm VCSEL array at such a low driving current. Our VCSEL array shows stable impulse response characteristics and uniform far-field spot morphology. © 2018 The Japan Society of Applied Physics

A vertical-cavity surface emitting laser (VCSEL) has unique advantages, such as the lack of catastrophic optical mirror damage (COMD), high modulation speed, monolithic array fabrication capability, and good beam-shape symmetry.[1–3] Moreover, VCSELs have been applied and developed in the fields of three-dimensional (3D) face recognition, light detection and ranging (LIDAR), and virtual reality/augmented reality (VR/AR) technology in recent years.[4–7] In these fields, VCSEL arrays composed of hundreds of lasing devices are used. VCSEL arrays can provide much higher laser powers than the conventional VCSELs used in optical communication systems. The application of high-power VCSEL arrays, especially in flash LIDAR, can help to achieve high-integration, compact optical systems at low cost and high volumes. Here, the intrinsic advantages of the unique VCSEL technology can prove its superiority.

Flash LIDAR systems are based on time-of-flight (TOF) depth sensing. The system combines a detector array with the measured return times from pulses of light to provide range information. Each pixel of the detector array measures a return time from its part of the field of view. Thus, the range information is added to provide the third dimension via a depth map. In most cases, the light source provides a single pulse per frame, resulting in a low duty cycle, but a high peak optical power is required. Typical pulse widths are in the ~1–25 ns range, and the repetition rate of the optical pulse may be up to 100 kHz. According to the actual requirements of LIDAR, VCSEL arrays for that purpose must support pulsed operation with narrow pulse widths and extremely low duty cycles. The laser peak power is required to reach dozens or even hundreds of watts to ensure a sufficiently large safe detection distance whilst ensuring eye safety. At present, most studies of VCSELs with a high peak power mainly concentrate on the 980 nm waveband. Since 2009, the laser power levels of the 980 nm VCSELs and its arrays have gradually increased from the initial 10 W[8] to 40 W and higher.[9] Subsequently, our team increased the 980 nm VCSEL single-emitter laser power to 92 W[10] and the VCSEL array laser power to 123 W.[11] In addition, the output power was increased to 210 W using four single emitters in a series structure.[12]

Although the 980 nm VCSEL achieved high laser power levels, the wavelength is unsuitable for the LIDAR system needed for intelligent driving. The 910 nm laser source is currently used in LIDAR to reduce water vapor absorption in the environment. Solutions in the long-wavelength regime[13] share the same properties here, but require expensive detectors whilst low-cost silicon detectors have the best response sensitivity in the 910 nm wavelength band.[14] However, the development of 910 nm VCSELs is challenging. For the 910 nm VCSEL, the Al content of the lower Al layer in the distributed Bragg reflector (DBR) should be larger than 10% to avoid the optical absorption risk at this wavelength. However, binary GaAs can be used as the lower Al layer in the DBR for the 980 nm VCSEL, which has larger thermal and electrical conductivities. Thus, the DBR material of the 910 nm VCSEL has to be adopted with a higher Al content in the high-refractive-index layer. This lowers the Al content difference together with the refractive-index contrast. Consequently, additional p-DBR pairs are needed to maintain the required DBR reflectivity to confine the optical wave. This generates higher ohmic resistance and optical absorption losses. In addition, the GaAs substrates used in the VCSEL growth have an optical absorption risk near the 910 nm. Therefore, a top emitting structure must be used. However, the lower conductivity of p-type materials together with the current aperture formed by oxidation with their curved current paths makes VCSELs prone to current crowding.[15] This can subsequently result in spatial hole-burning and a nonuniform optical field distribution. To avoid the current crowding effect, the mesa dimension of a top-emitting VCSEL is usually less than 50 μm. However, for the 980 nm VCSEL with the bottom emitting structure, the mesa dimension of more than 100 μm can be used. Also, a more efficient heat removal can be realized for the bottom emitting structure because of the very close distance between the active region and the heat sink.

Thus far, only Carson and colleagues of Trilumina Company have reported the preliminary achievement of high-peak-power VCSELs dedicated to long-distance LIDAR.[16,17] In their paper, a 1 × 5 sectored VCSEL array module at 905 nm is presented. When the driving current of their array module is 100 A, the output power is approximately 80 W,[17]

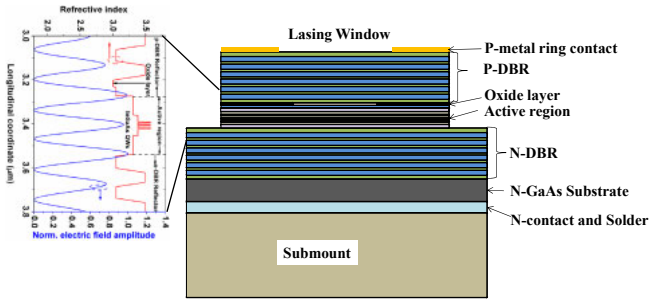

Fig. 1. (Color online) Schematic diagram of 910 nm VCSEL cross-sectional structure and the distribution of standing wave near the active area (inset).

and the maximum slope efficiency is approximately 1.4 W/A only. Hence, a significant increase in operating current is required to achieve a higher laser output power. A high operating current and its high bias voltage would undoubtedly increase the risk of electric breakdown of the VCSEL array, which can seriously affect the working reliability of the array. In addition, achieving a driving current of hundreds of amperes is difficult with a highly integrated laser LIDAR driving power supply module. Therefore, achieving high peak power at the lowest laser current is one of the key requirements for the LIDAR system application of VCSEL arrays.

In this paper, we present our latest achievements in fabricating high-peak-power 910 nm VCSEL arrays with a low operating current and its sectored array modules. Firstly, we discuss the optimization of a high-peak-power 910 nm VCSEL array and explain the selection principle of the technological parameters. Secondly, after presenting the laser power characteristics of our VCSEL arrays, we analyze power saturation phenomena in the power–current curve by spectral measurement and compare the optical pulse waveforms of the sectored array under different operating currents. Finally, we verify the beam shaping of the sectored array using an external optical collimator lens. We could achieve a peak power exceeding 100 W with operating currents as low as 55 A.

The schematic diagram of the epitaxial structure of our 910 nm VCSEL is shown in Fig. 1. The structure consists of an *n*-doped lower DBR structure, an active region, and a p-doped top DBR structure. The active region is composed of three 6 nm $In_{0.11}Ga_{0.89}As$ quantum wells (QWs) and 8 nm $Al_{0.3}Ga_{0.7}As$ barrier layers. The optical thickness of the active region is one λ in wavelength. For high optical gain, the three QWs are located at the center of the standing wave peak in the structural design (Fig. 1). The carbon-doped p-type Bragg reflector consisted of 20 pairs of $Al_{0.12}Ga_{0.88}As/Al_{0.9}Ga_{0.1}As$ layers. For selective oxidation, a 30-nm-thick $Al_{0.98}Ga_{0.02}As$ layer was partially used instead of the $Al_{0.9}Ga_{0.1}As$ layer, near the active region, in the p-side DBR. The $Al_{0.98}Ga_{0.02}As$ layer is then selectively oxidized to form an oxide aperture for current-and-transverse optical mode confinement. The 34-period n-mirror below the active region was Si-doped. A top lasing structure was adopted for the VCSEL structure to avoid optical absorption by the GaAs substrate. We defined the p-metal ring contact together with the lasing window by a metal lift-off process. The thickness of the substrate is reduced to be 150 μm before depositing the n-type contact metal.

For our top emission VCSEL array, we reduced the number of p-DBR pairs to 20 to achieve high slope efficiency

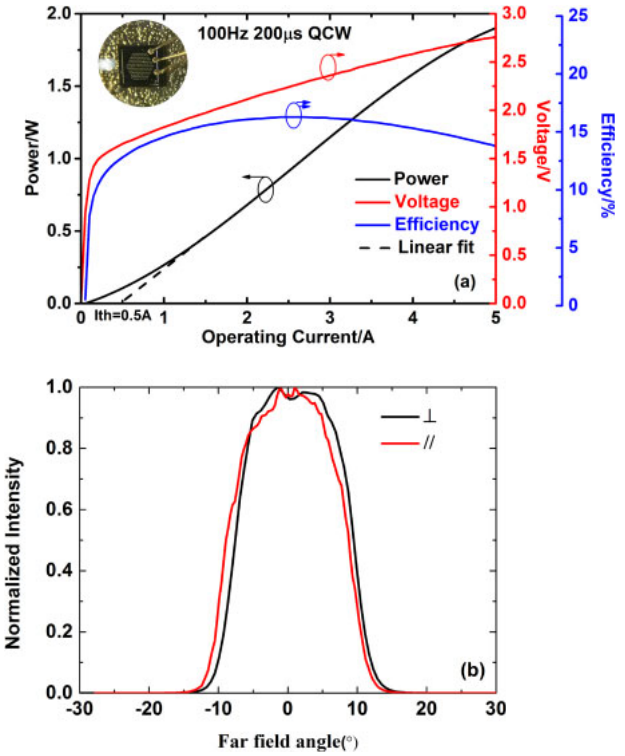

Fig. 2. (Color online) Quasi-CW (100 Hz, 200 μs) characteristics of the 163-device VCSEL array. (a) Laser output power, wall-plug efficiency, and voltage versus driving current (inset: photograph of the mounted VCSEL array). (b) Far-field divergence angle of the array parallel and perpendicular to the wafer crystal.

and output power. This method can also effectively reduce its resistance. To ensure a high dynamic response with superior pulse output characteristics of the VCSEL array, we optimized the dimensions of the oxide aperture and the electrode aperture of the single emitter within the array[18,19] to obtain the highest element slope efficiency together with a low threshold current. Finally, we determined the optimal geometry of the oxide aperture and top contact window of the VCSEL array elements to be 8 and 15 μm, respectively. The mesa diameter is 30 μm and the array has a pitch of 50 μm. Given the parallel geometry, power scales with the elements of the VCSEL array.[20] Therefore, we integrated as many solitary VCSEL elements as possible in the array. At the same time, this reduces the parasitic inductance effect of the whole array.[20] To ensure the most similar working state among the elements and ensure the uniformity of the VCSEL array, we fabricated a VCSEL array structure with luminescent elements arranged in a hexagonal honeycomb shape. The total number of luminescent elements in the array is 163 (a total active area of 8189 μm^2).

To verify the optimization effect of the above epitaxial structure and process structure, we tested the working characteristics of the fabricated VCSEL array under the quasi-continuous driving of 100 Hz and 200 μs. The test results are shown in Fig. 2. Before the test, we packaged the VCSEL array briefly and completed the gold wire bonding. No heat dissipation is applied during the test. Figure 2(a) depicts the relation curve between the single-array laser power, voltage, efficiency, and operating current. The threshold current is 0.5 A. When the VCSEL array achieves nearly 2 W output power, the slope efficiency is approximately 0.45 W/A, and

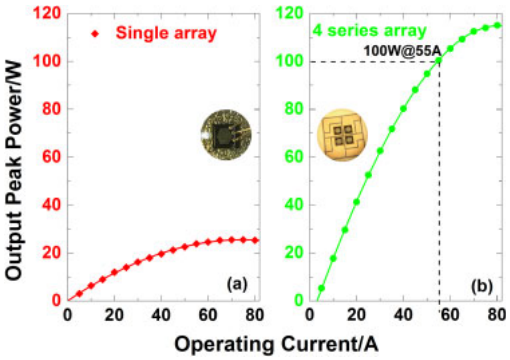

Fig. 3. (Color online) Laser output power versus driving current under a repetition frequency of 10 kHz and a pulse width of 30 ns. (a) For the single 163-device 910 nm VCSEL array and (b) for the sectored VCSEL array with all of the 4 arrays connected in a 2×2 form lasing. The insets show photos of the mounted VCSEL arrays measured.

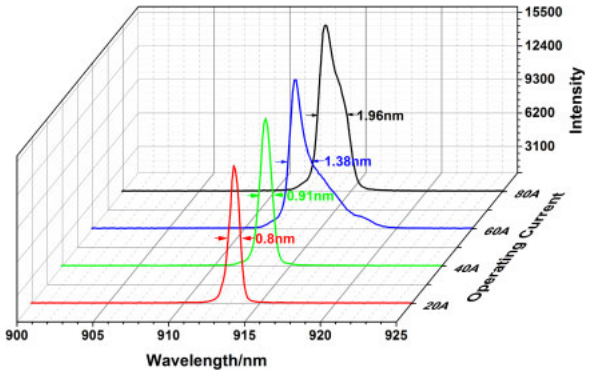

Fig. 4. (Color online) Laser spectra of the sectored VCSEL array under different driving currents in pulsed operation.

the power curve does not show a thermal rollover yet. The far-field divergence angle of the array is tested by the far-field scanning CCD system that we built. As depicted by the far-field divergence angle test results in Fig. 2(b), the optical fields of the VCSEL arrays in the two orthogonal directions are similar, and the divergence angles (FWHM) are 16.2 and 16.8°, which indicates that our array has a circular far-field symmetry. The distribution of optical intensity near the peak value in the curve is relatively smooth. Hence, all the elements in the VCSEL array emit uniformity, and good optical field collimation can be expected in practical applications.

The relationship between the single VCSEL array peak power and the operating current is measured under the pulsed driving conditions with a repetition frequency of 10 kHz and a pulse width of 30 ns [Fig. 3(a)]. When the operating current reaches 40 A, the peak power of the VCSEL array is 20 W. As the operating current further increases, the peak laser power of the single VCSEL array reached a maximum of 25.5 W at the operating current of 80 A.

We adopted a four-element sectored module structure[11] reported previously to fabricate a larger VCSEL array subdivided into 2×2 individually addressable sectors. Sectors are covered by the graphical Au electroplating on the AlN submount. Then, the submount is fixed by the designed fixture tools and the solder is evaporated on the sector region. The four VCSEL arrays are packaged on this submount by the reflow soldering. With this array, we realized even higher laser powers at a low driving current. The pulsed laser characteristics of the sectored VCSEL array modules are shown in Fig. 3(b). Under the same operating current, the laser output power of the sectored VCSEL array module is approximately four times that of a single VCSEL array, and the maximum slope efficiency reaches 1.8 W/A. These results indicate that our VCSEL arrays were fabricated with high yield and good homogeneity. Under pulsed driving conditions comparable to those of our single array, the output power of the sectored VCSEL array module reached 100 W under the operating current of 55 A. To the best of our knowledge, this is the first report on a 910 nm VCSEL module achieving the 100 W output power level at such a low driving current. The peak laser power of the large sectored VCSEL array reaches its maximum of 115 W at an operating current of 80 A.

The laser output power curves of the single array and the sectored module demonstrate an obvious power saturation phenomenon at high driving currents (Fig. 3). This phenomenon confirms that the laser power of the VCSEL array cannot be increased infinitely with the increase in driving current even at extremely low duty cycle pulse driving currents. Subsequently, we analyzed the reason for the VCSEL power saturation through the spectral characteristics of the large sectored VCSEL array.

The variation of the laser spectra of the VCSEL array under different driving currents is presented in Fig. 4. The laser spectra show clear spectrum broadening with an increase in operating current. When the driving current increased from 20 to 80 A, the spectral width increased from 0.8 to 1.96 nm while the peak wavelength hardly changed. The spectral broadening phenomenon is consistent with previously reported VCSEL array research results[9] being attributed to thermal crowding within the VCSEL array. On the basis of the temperature coefficient of 0.06 nm/K,[20] the average internal temperature rise of the VCSEL arrays is estimated to be 20 K at 80 A driving current. Thus, the center part of each array would experience several increases in temperature, according to the thermal crosstalk model of VCSEL arrays developed by Amann and Hofmann.[21]

The above phenomena indicate that the VCSEL array can generate a serious internal thermal effect even under narrow pulse driving current, owing to the high thermal time constants. Moreover, a high carrier density is formed in the active region of VCSEL array elements under large operating currents inducing serious carrier leakage within QWs at high temperatures,[22,23] causing the output power to saturate. To sum up, for a high efficiency VCSEL module required by the applications, achieving high output power together with low driving currents is both challenging and essential.

The optical pulse output waveform of the VCSEL array characterizes its pulse response characteristics under narrow pulse driving conditions, which can directly affect the time measurement accuracy of the LIDAR. We have developed the external power supply by ourselves to investigate the stability of our VCSEL arrays at different driving currents. As is known, it is very difficult to achieve a driving power supply with both a current of nearly 100 A and a nanosecond pulse width. Thus, for comprehensive consideration, we developed a power supply with a pulse width of 30 ns and a maximum driving current of 80 A. In this work, the pulse width of 30 ns

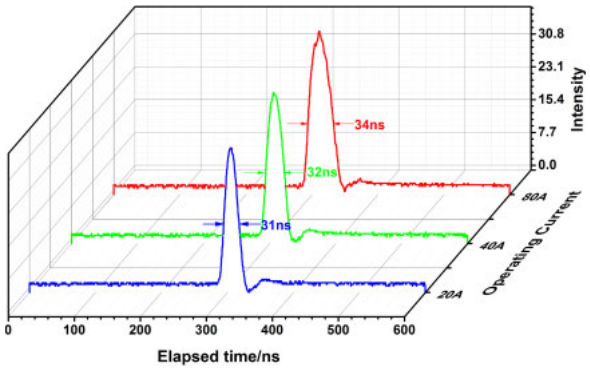

Fig. 5. (Color online) Comparison of the optical pulse waveforms of the sectored VCSEL array at different working currents.

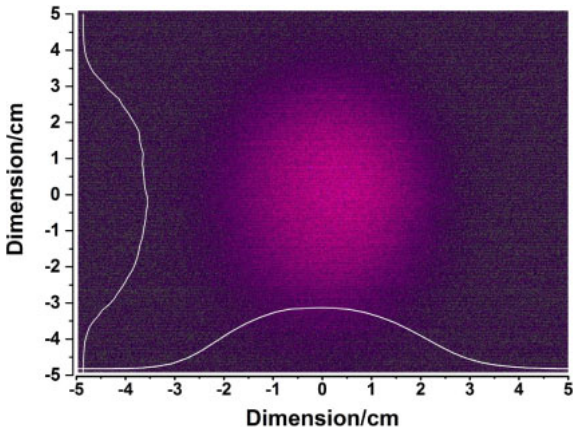

Fig. 6. (Color online) Far field at 1 m distance of the sectored VCSEL array, all four sectors operating, beam collimation with a single spherical collimator lens.

is slightly larger than the required pulse width of the LIDAR. However, the purpose of our test in this work is simply just to verify the stability of the pulse response with the increase in driving current. Therefore, a photodetector and an oscilloscope system are used to capture the optical pulse waveform of our VCSEL arrays.

The optical pulse waveforms of the large VCSEL array under different driving currents are shown in Fig. 5. The array exhibits a smooth optical pulse waveform signal. Different from previous reports,[20,24] no serious tailing phenomenon appears in our optical pulse waveform. Instead, a negative signal overshoot emerges, which soon returns to zero. Given that all solitary VCSEL devices of the array are operated in parallel, we observe a lower inductance effect of our high-density VCSEL array[21] than of the VCSEL arrays with only a few elements as reported previously. This design eliminates the trailing effect of the optical pulse waveform driven by narrow pulses. When the driving current of our sectored array is increased from 20 to 80 A, the half width of the pulse waveform is widened from 31 to 34 ns, and the width is widened by 3 ns (Fig. 5). The weak broadening of the optical pulses at a high current is probably caused by internal heating at a high current.[20] Although the optical pulse exhibits weak broadening at a high current, the pulse waveforms of the array under different driving currents still have a good pulse shape (Fig. 5). The pulse stability shown by the large sectored VCSEL array mentioned above is extremely important for realizing the stable operation of the LIDAR in different environments.

For the following collimating and beam shaping experiments, we intentionally omitted costly lens arrays.[25,26] Instead, we directly used a conventional spherical collimator of 100 mm focal length and 50 mm diameter to verify whether our arrays can be applied in automotive solutions with high cost pressure and high reliability requirements. We adjusted the collimator lens position to optimize the collimation effect. To monitor the far field, we put a coarse plastic screen approximately 1 m away from the collimator lens, and then used the CCD to capture the optical field morphology as presented in Fig. 6. The collimated far-field light spot shows a circular symmetrical shape, and the intensity distribution of the light field gradually decreases from the central region to the edge. The diameter of the spot 1 m distance from the lens is about 6–7 cm. No dark spot was found in the entire light field region. This outcome is similar to the far field distribution morphology of the small VCSEL array as presented in Fig. 2(b), which indicates that we achieved consistent far-field spot morphology also with our compact 2 × 2 sectored and addressable array modules.

We reported our latest achievements on high-peak-power 910 nm VCSEL arrays, which can be successfully fabricated in large sectored configurations. These arrays are an ideal laser source for application in LIDAR. We realized a pulse output power of 25.5 W for a single VCSEL array of 163 VCSELs operating in parallel. On the basis of the above analysis, an addressable four-sector VCSEL array with a 2 × 2 configuration was developed in this study. The maximum slope efficiency of that array is 1.8 W/A, and the maximum power reached 115 W. At a driving current of only 55 A, we could already demonstrate an optical output exceeding 100 W. An analysis of the spectral broadening of the sectored array confirms that internal thermal effect and carrier leakage are the main reasons for the power saturation of the laser peak power at a high current. Such finding verifies the necessity of the VCSEL array to achieve a high peak power output at a low current. Targeting low-cost automotive solutions, we directly used a single spherical lens as collimation optics of the sectored array demonstrating a nearly Gaussian-shaped far field with high uniformity and circular symmetry. Given its advantages of low operating current, high peak power, good pulse waveform, and easy collimation, we believe that this VCSEL array can substantially reduce the cost of existing laser radar systems, improve the integration and measurement distance of such systems, and hasten the arrival of the future intelligent driving era.

Acknowledgments This work was supported by the National Key Research and Development Program of China (No. 2017YFB0503200), Fudan University-CIOMP Joint Fund (No. FC2017-002), National Natural Science Foundation of China (Nos. 61434005, 11674314, 11774343, and 61727822), Chinese Academy of Sciences President's International Fellowship Initiative (Grant No. 2018VTA0005), and Key Projects of Jilin Province Science and Technology Development Plan (Nos. 20180201119GX, 20160414016GH, and 20160204073GX).

1) S. Inoue, S. Nishimura, M. Nakahama, A. Matsutani, T. Sakaguchi, and F. Koyama, Jpn. J. Appl. Phys. **57**, 040308 (2018).
2) B. W. Tilma, M. Mangold, C. A. Zaugg, S. M. Link, D. Waldburger, A. Klenner, A. S. Mayer, E. Gini, M. Golling, and U. Keller, Light: Sci. Appl. **4**, e310 (2015).

3) K. Iga, Jpn. J. Appl. Phys. **47**, 1 (2008).
4) H. Moench, M. Carpaij, P. Gerlach, S. Gronenborn, R. Gudde, J. Hellmig, J. Kolb, and A. Lee, Proc. SPIE **9766**, 97660A (2016).
5) J. F. Seurin, D. Zhou, G. Xu, A. Miglo, D. Li, T. Chen, B. Guo, and C. Ghosh, Proc. SPIE **9766**, 97660D (2016).
6) D. Zhou, J.-F. Seurin, G. Xu, P. Zhao, B. Xu, T. Chen, R. Van Leeuwen, J. Matheussen, Q. Wang, and C. Ghosh, Proc. SPIE **9381**, 93810B (2015).
7) M. S. Wei, F. Xing, and Z. You, Light: Sci. Appl. **7**, 18006 (2018).
8) N. Otake, K. Abe, H. Yamada, H. Wado, and Y. Takeuchi, Appl. Phys. Express **2**, 052102 (2009).
9) H. Naito, M. Miyamoto, Y. Aoki, A. Higuchi, K. Torii, T. Nagakura, T. Morita, J. Maeda, H. Miyajima, and H. Yoshida, Appl. Phys. Express **5**, 082104 (2012).
10) L. Zhang, Y. Ning, Y. Zeng, L. Qin, Y. Liu, X. Zhang, D. Liu, H. Xu, J. Zhang, and L. Wang, Appl. Phys. Express **4**, 052102 (2011).
11) D. Liu, Y. Ning, Y. Zeng, L. Qin, Y. Liu, X. Zhang, L. Zhang, J. Zhang, C. Tong, and L. Wang, Appl. Phys. Express **4**, 052104 (2011).
12) J. Zhang, Y. Ning, X. Zhang, J. Zhang, Y. Zeng, X. Shan, L. Qin, and L. Wang, Jpn. J. Appl. Phys. **53**, 070303 (2014).
13) W. Hofmann, M. Görblich, M. Ortsiefer, G. Böhm, and M. C. Amann, Electron. Lett. **43**, 1025 (2007).
14) A. Samman, L. Rimai, J. R. McBride, R. O. Carter, W. H. Weber, C. Gmachi, F. Capasso, A. L. Hutchinson, D. L. Sivco, and A. Y. Cho, 5th IEEE-VTS Fall VTC, 2000, p. 2084.
15) X. Zhang, Y. Ning, Y. Zeng, J. Zhang, X. Fu, L. Qin, Y. Liu, C. Tong, and L. Wang, IEEE J. Quantum Electron. **48**, 42 (2012).
16) M. E. Warren, R. F. Carson, J. R. Joseph, T. Wilcox, P. Dacha, D. J. Abell, and K. J. Otis, Proc. SPIE **9381**, 93810C (2015).
17) R. F. Carson, M. E. Warren, P. Dacha, T. Wilcox, J. G. Maynard, D. J. Abell, and K. J. Otis, Proc. SPIE **9766**, 97660B (2016).
18) J. F. Seurin, G. Xu, V. Khalfin, A. Miglo, J. D. Wynn, P. Pradhan, C. L. Ghosh, and L. A. D. Asaro, Proc. SPIE **7229**, 722903 (2009).
19) A. P. Engelhardt, J. S. Kolb, F. Roemer, U. Weichmann, H. Moench, and B. Witzigmann, Proc. SPIE **9381**, 93810M (2015).
20) A. Higuchi, H. Naito, K. Torii, M. Miyamoto, J. Maeda, H. Miyajima, and H. Yoshida, Opt. Express **20**, 4206 (2012).
21) M. C. Amann and W. Hofmann, IEEE J. Sel. Top. Quantum Electron. **15**, 861 (2009).
22) Y. Arakawa and A. Yariv, IEEE J. Quantum Electron. **22**, 1887 (1986).
23) R. G. Ispasoiu, A. M. Fox, and D. Botez, IEEE J. Quantum Electron. **36**, 858 (2000).
24) H. Naito, M. Miyamoto, Y. Aoki, A. Higuchi, K. Torii, T. Nagakura, T. Morita, J. Maeda, H. Miyajima, and H. Yoshida, Proc. SPIE **8639**, 86390N (2013).
25) H. Moench, C. Deppe, R. Dumoulin, S. Gronenborn, X. Gu, G. Heusler, M. Miller, P. Pekarski, and A. Pruijmboom, Proc. SPIE **8241**, 82410B (2012).
26) X. Yin, T. Steinle, L. Huang, T. Taubner, M. Wuttig, T. Zentgraf, and H. Giessen, Light: Sci. Appl. **6**, e17016 (2017).